

UC Davis

UC Davis Previously Published Works

Title

Fluorescent “Turn off-on” Small-Molecule-Monitoring Nanoplatform Based on Dendrimer-like Peptides as Competitors

Permalink

<https://escholarship.org/uc/item/97x069m2>

Journal

ACS Applied Materials & Interfaces, 11(36)

ISSN

1944-8244

Authors

Chen, He
Ding, Yuan
Yang, Qian
[et al.](#)

Publication Date

2019-09-11

DOI

10.1021/acsami.9b13111

Peer reviewed



Published in final edited form as:

ACS Appl Mater Interfaces. 2019 September 11; 11(36): 33380–33389. doi:10.1021/acsami.9b13111.

Fluorescent “Turn off-on” Small-Molecule-Monitoring Nanoplatfom Based on Dendrimer-like Peptides as Competitors

He Chen^{†,‡}, Yuan Ding^{†,‡}, Qian Yang^{†,‡}, Bogdan Barnych[§], Gualberto González-Sapienza[⊥], Bruce D. Hammock[§], Minghua Wang^{†,‡}, Xiude Hua^{*,†,‡}

[†]College of Plant Protection, Nanjing Agricultural University, Nanjing 210095, China

[‡]State & Local Joint Engineering Research Center of Green Pesticide Invention and Application, Nanjing 210095, China

[§]Department of Entomology and Nematology and UCD Cancer Center, University of California, 96 Briggs Hall, Davis, California 95616, United States

[⊥]Cátedra de Inmunología, Facultad de Química, Instituto de Higiene, Universidad de la República, Montevideo 11600, Uruguay

Abstract

Peptides isolated from phage display libraries are powerful reagents for small-molecule immunoassay; however, their application as phage-borne peptides is significantly limited by the biological nature of the phage. Here, we present the use of lysine scaffold to prepare a series of different valence peptides to serve as replacements for phage-borne peptides. Benzothiostrubin was selected as a model analyte, the cyclic benzothiostrubin-peptidomimetic in the form of monomer, dendrimer-like dimer, and tetramer were designed and synthesized. Compared with the monomer, the affinity of dendrimer-like dimer and tetramer increased 1.87 and 13.6 times, respectively, as determined by isothermal titration calorimetry (ITC). A novel inner filter effect immunoassay (IFE-IA) with positive readout was developed for benzothiostrubin detection utilizing the peptidomimetics attached to upconversion nanoparticles (UCNPs) as energy donor and monoclonal antibody (mAb)-labeled urchin-like gold nanoflowers (AuNFs) as energy absorber, respectively. The sensitivity of the assay based on dendrimer-like tetramer was approximately 6 and 3 times higher than monomer and dendrimer-like dimer, respectively. After optimization, 50% saturation of the signal (SC_{50}) and detection range (SC_{10} to SC_{90}) of the IFE-IA based on dendrimer-like tetramer were 11.81 ng mL^{-1} and $2.04\text{--}106.17 \text{ ng mL}^{-1}$, respectively. The IFE-IA also shows good accuracy for the detection of benzothiostrubin in authentic samples.

Graphical Abstract

*Corresponding Author huaxiude@njau.edu.cn. Tel.: +86 25 84395479. Fax: +86 25 84395479.

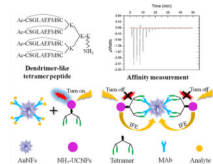
ASSOCIATED CONTENT

Supporting Information

The Supporting Information is available free of charge on the ACS Publications website at DOI: [10.1021/acsami.9b13111](https://doi.org/10.1021/acsami.9b13111).

Purity and measured molecular weight of peptides (Table S1), the amounts of benzothiostrubin detected by IFE-IA and HPLC simultaneously (Table S2), validation of peptides by ic-ELISA (Figure S1), optimization of working buffer parameters (Figure S2), matrix interference of samples in IFE-IA (Figure S3) (PDF)

The authors declare no competing financial interest.



Keywords

dendrimer-like peptide; peptidomimetic; inner filter effect; upconversion nanoparticles; gold nanoflowers

1. INTRODUCTION

Phage-displayed peptide libraries are powerful tools for the rapid selection of phage-borne peptides that specifically bind to antibodies (peptidomimetic) and immunocomplexes (anti-immunocomplex) of small molecules.¹ There are two attractive alternative approaches for the measurement of small molecule analytes by using phage-borne peptides. The first one is competitive,^{2–5} where peptidomimetic is used as substitute for hapten or analyte to develop competitive immunoassays with increased sensitivity. The other is noncompetitive,^{6–10} in which anti-immunocomplex peptides specifically bind with the analyte-antibody immunocomplex to improve specificity of the assay. However, the active peptides linked to phage coat protein have limited use in immunoassay field caused by the large size of phage particle (880 × 6–7 nm), poor fluidity, and potential biohazard.^{5–10} Additionally, they are inconvenient reagents for the development of homogeneous and one-step immunoassays due to difficulties associated with labeling of phage particles. Thus, research on substitutes for phage-borne peptides is of great significance.

Synthetic peptides chemically coupled to nanoparticles,^{11,12} streptavidin,¹³ or fluorescein isothiocyanate (FITC),^{14,15} as well as peptides recombinantly fused with emerald-green fluorescent protein (EmGFP),¹⁶ streptavidin,¹⁷ or nano luciferase (NanoLuc),⁵ have been proven to be useful reagents for phage-free immunoassays. Synthetic peptides as more convenient, higher purity, easier to modify and control materials compared to recombinant peptide—protein chimeras are more widely used for small molecule compound immunoassays.^{13,15} However, peptides derived from phage display often suffer from poor binding affinity caused by the reduction in the number of copies (the overall avidity of phage-borne peptides were replaced by lower affinity monomer), which is unsatisfactory for the development of highly sensitive immunoassays.^{13–18} Vanrell et al. showed that monovalent biotinylated peptides derived from phage display, do not bind the molinate-antibody immunocomplex; however, the binding is recovered for tetravalent streptavidin-peptide complex.¹⁷ Li et al. assembled a multivalent peptide ligand, which showed higher affinity and specificity than the monovalent ligand.¹⁹ Helms and Dudak also demonstrated that the valence of peptide ligands plays an important role in affinity toward receptors through dendrimer display.^{20,21} Up to now, pentavalent dendritic platform,²⁰ multivalent small-molecule- decorated nanomaterials,²² decameric water-soluble carbohydrate ligand,²³ and multivalent polyethylene glycol platform with chondrocyte affinity peptide²⁴ have been

reported to enhance the affinity of ligands or bioreceptor and provide reliable technical support for the study of dendrimeric peptides.

Several homogeneous immunoassays with positive readout have been reported for small molecule monitoring by a turn off-on model, such as immunoassays based on the bioluminescence resonance energy transfer (BRET),²⁵ fluorescence resonance energy transfer (FRET)²⁶ and inner filter effect (IFE).²⁷ In these immunoassays, the signal is directly proportional to the concentration of the analyte, which helps to produce a more intuitive readout. IFE is a nonirradiation energy conversion model in which the excitation and/or emission light is absorbed by absorbers in spectrofluorometry. IFE-based immunoassays are more attractive compared to BRET or FRET due to reduced development requirements (IFE also can occur if distances between donor and quencher exceed 10 nm).²⁸ Upconverting nanoparticles (UCNPs) are lanthanide-doped nanomaterials, which could emit high visible light under excitation by near-infrared (NIR) radiation. They have been widely used as energy donors in immunoassays because of the large anti-Stokes shift, high photostability, little background fluorescence and light scattering.^{29–33} In addition, gold nanoparticles are excellent energy acceptors in the visible domain caused by the large molar absorptivity. Compared with gold nanospheres (AuNSs) and gold nanorods (AuNRs), urchin-like gold nanoflowers (AuNFs) show higher optical extinction due to the electromagnetic field enhancement at the branched tips.³⁴ Additionally, they have a larger specific surface area resulting in improved protein immobilization yield and better colloid-stability than the same size AuNSs, AuNRs. To date, AuNFs have been extensively used in chemical and biological analysis.^{35,36}

Benzothiostrubin is a novel strobilurin fungicide, which shows excellent disease control in crops, especially for powdery mildew and downy mildew.³⁷ In our previous study, a phage-borne peptide (CSGLAEFMSC, C3–3) specifically binding to an antibenzothiostrubin monoclonal antibody (mAb) was isolated from a cyclic 8-residue peptide phage library. In this paper, monomer (Ac-CSGLAEFMSCK), dendrimer-like dimer ((Ac-CSGLAEFMSC)₂KK) and tetramer (((Ac-CSGLAEFMSC)₂K)₂KK) peptidomimetics were designed and synthesized through reconstruction of the phage-borne peptidomimetic of benzothiostrubin using special scaffolds and spacer (Scheme 1A). The affinities between peptidomimetics of different valence and the mAb were measured by isothermal titration calorimetry (ITC). Additionally, a turn off-on immunoassay for benzothiostrubin was proposed based on IFE by using dendrimer-like peptide-conjugated UCNPs as donor and mAb-labeled AuNFs as absorber (Scheme 1B).

2. EXPERIMENTAL SECTION

2.1. Reagents and Apparatus.

Rare earth oxides, including yttrium oxide (Y₂O₃ > 99.9%), ytterbium oxide (Yb₂O₃ > 99.9%), erbium oxide (Er₂O₃ > 99.9%), NaF, (3-aminopropyl)-triethoxysilane (APTES, 98%), tetraethyl orthosilicate (TEOS, 98%), trihydroxymethyl aminomethane (Tris) (99.9%) were purchased from Aladdin Industrial Corporation (Shanghai, China). Chloroauric acid (HAuCl₄·4H₂O, > 99.9%) and 25% glutaraldehyde solution were purchased from Sinopharm Chemical Reagent Co., Ltd. (Shanghai, China). Sodium

tetraborate ($\text{Na}_2\text{B}_4\text{O}_7 \cdot 10\text{H}_2\text{O}$) was purchased from Lingfeng Chemical Reagent Co., Ltd. (Shanghai, China) and all experiments were carried out in its aqueous buffer (BB, 0.05 M, unless indicated otherwise). Antibenzothioistrobin mAb 4E8 was prepared previously in our laboratory.³⁸ The phage-displayed peptidomimetic (C3–3, CSGLAEFMSC) was previously isolated from a cyclic 8-amino-acid random peptide library.⁹ Monomer (Ac-CSGLAEFMSC), dendrimer-like dimer ((Ac-CSGLAEFMSC)₂KK) and tetramer (((Ac-CSGLAEFMSC)₂K)₂KK) were synthesized and purified by Apeptide Co., Ltd. (Shanghai, China).

Affinity of mAb and peptides were detected by MicroCal iTC200 (Malvern Instruments, Worcestershire, UK). The morphology of UCNPs and AuNSs were characterized by transmission electron microscopy (TEM, H-7650, Japan) and the AuNFs were characterized by field emission scanning electron microscope (SEM, S-4800, Japan). The crystal structure and surface chemistry of UCNPs were tested using a X-ray diffractometer (XRD, D8 Advance, Bruker, Germany) and Fourier transform infrared spectrometer (FTIR, Bruker Vector-22, Germany), respectively. Fluorescence intensity of UCNPs was recorded by F-2700 fluorescence photometer (Hitachi Ltd., Japan) with an external 980 nm laser source (Changchun Laser Optoelectronics Technology Co., Ltd., China). The fluorescence lifetime was detected by LS 55 fluorescence spectrometer with a 980 nm laser source (PerkinElmer, America). Benzothioistrobin was detected using an Agilent 1260 HPLC with UV detector (serial number: G1314F), quat pump (serial number: G1311C) and auto sampler (G1329B) (Santa Clara, CA, USA).

2.2. ITC Measurements.

ITC measurements were implemented to study the thermodynamic characteristics of the interaction between peptides with different valence and mAb. The calorimetric titrations were performed at 25 °C. All samples were diluted by 10 mM BB and degassed prior to use. The sample cell was filled with 6.7, 10, and 10 μM mAb solution (400 μL) for monomer, dendrimer-like dimer and tetramer respectively, while 10 mM BB was set as a control. Double-distilled water was added into the reference cell. Solutions (100 μL) of 260 μM monomer, 150 μM dimer, or 50 μM tetramer in PCR tube were placed on the load position. After automatic loading of the peptide solution, the sampler was moved to a sample cell. The parameter of total injections, initial delay time and stirring speed were set as 20, 60 s, and 1000 rpm, respectively. Under the dynamic correction mode, the heat released with titrations was detected by calorimeter, the stoichiometry (N), binding constants (K , reciprocal of affinity constant (K_D), binding enthalpy (H), entropy (S) were determined by the Origin software fitting with an OneSites model. The c value, which was calculated according to the formula $c = M_{\text{tot}}N/D$ (N represents the binding stoichiometry, M_{tot} represents the molar concentration of sample molecule in the cell, D represents the affinity constant), was used to ensure the quality of the results.

2.3. Preparation and Verification of Probes.

2.3.1. Preparation and Verification of AuNFs and mAb-Labeled AuNFs.—The AuNFs were synthesized according to a gold seed-mediated growth approach^{34,36} with a slight modification. Briefly, 100 mL of ultrapure water containing 0.01% HAuCl_4 was

heated to boiling, and then 3 mL of 1% sodium citrate solution was added with vigorous stirring. After the solution color turns from mazarine to wine red, the mixture was heated for additional 5 min and naturally cooled to room temperature (RT) and stored at 4 °C to use as seed crystals. For the larger AuNFs, 300 μ L of 1% HAuCl₄, 150 μ L of gold seeds, 110 μ L of 1% sodium citrate solution, and 500 μ L of 0.03 M hydroquinone were added sequentially to 50 mL of ultrapure water with stirring for 30 min at room temperature.

The AuNF probes (mAb-labeled AuNFs) were prepared by the Rafael method.³⁹ Briefly, 500 mL of AuNFs was adjusted to pH 10.0 with 0.2 M K₂CO₃, and 1.25 mg of mAb was added with gentle stirring for 1 h at RT. The remaining active sites were blocked with 10% BSA for another 1 h and the free mAb were removed by centrifuging at 3000 *g* for 15 min, the precipitate was redissolved in 25 mL 0.01 M BB and stored at 4 °C until use. Finally, AuNFs and AuNF probes were characterized by spectroscopy and zeta potential.⁴⁰

2.3.2. Preparation and Verification of UCNPs, Amino-Modified UCNPs, and Peptide-Labeled UCNPs.—

The NaYF₄:Yb,Er UCNPs were synthesized by the hydrothermal method.⁴¹ Briefly, 63.3 mg of Y₂O₃, 276.6 mg of Yb₂O₃, 7.6 mg of Er₂O₃, and 60 mL of concentrated nitric acid were heated to clarification and dryness in a florence flask. The dry powder was dissolved in 6 mL of ultrapure water with ultrasonication for 5 min, and 2 mL of 0.7 M sodium citrate was added with stirring for about 10 min. Next, 24 mL of 1.1 M NaF was added dropwise, the pH was adjusted to 5.0, and the resulting solution was kept stirring for 2 h. Finally, the mixture was transferred to an autoclave and heated at 205 °C for 12 h. After cooling and centrifugation, the precipitate was washed by ultrapure water and ethanol three times, respectively. The obtained UCNPs were dried at 60 °C and characterized by TEM and XRD.

Surface amino-functionalization of the UCNPs was carried out by the typical Stober-based method.⁴² Briefly, 40 mg UCNPs were ultrasonicated and vigorously stirred in 120 mL of isopropanol, every step lasting 30 min. Then, the suspension was transferred into incubator for another 10 min under 35 °C, 5 mL of ammonia solution, and 40 g of ultrapure water was added into the solution under rapid agitation. Next, 40 mL of isopropanol containing 50 μ L of TEOS was added dropwise to the above solution, and the mixture was stirring for 5 h. Finally, 60 mL of isopropanol containing 400 μ L of APTES was added dropwise and the reaction was allowed to proceed for another 1 h. Thereafter, the functionalized UCNPs were collected by centrifugation and washing with ultrapure water and ethanol for several times. The precipitate was dried and stored at 4 °C. The amino-modified UCNPs were validated by FTIR.

UCNP probes (peptide-labeled UCNPs) were prepared by the glutaraldehyde method.^{27,37,43} One hundred milligrams of amino-functionalized UCNPs were dispersed in 25 mL of 0.01 M BB by ultrasonication for 30 min. Subsequently, 500 mg of sodium borohydride and 6.4 mL glutaraldehyde aqueous solution (25%) were added and the reaction was shaken for 1 h at room temperature. After centrifugation and washing three times, the precipitate was redispersed in 50 mL of BB, 400 nmol of peptidomimetic, and 500 mg of sodium borohydride were added into the mixture with shaking for another 1 h. The unreacted sites were blocked by 500 mg Tris for 1 h. The UCNP probes were collected after centrifugation

and washing. Finally, the probes were dispersed into 25 mL BB and stored at 4 °C. Labeling of UCNP probes with murine antibody was validated using goat antimouse IgG-HRP. Briefly, 50 μL of UCNP probes, 2 μg of antibenzothiostrubin mAb was added to 2 mL tubes and adjusted to 1 mL by BB. The mixture was incubated 1 h at 37 °C. After centrifugation at 4000 *g* and washing with BB, the precipitate was resuspended in 500 μL of goat antimouse IgG-horse radish peroxidase (HRP) (1:20000 in BB) and incubated for another 1 h. The free goat antimouse IgG-HRP was removed by centrifugation, and 500 μL substrate solution was added for the detection of bound enzyme (HRP).

2.4. IFE-IA Protocols.

Monomer, dendrimer-like dimer, and tetramer peptidomimetics were applied to immunoassay with the same protocol and the immunoassay with lowest 50% saturation of the signal (SC50) was considered the most sensitive. Briefly, 500 μL of standard or sample solution, 50 μL of UCNP probes, and 60 μL of AuNF probes were added into a 2 mL tube and adjusted to 1 mL by BB. After incubation at 37 °C with a gentle shaking for 1 h, the suspension was transferred into a cuvette, and the fluorescence intensity at 657 nm was measured by using an F-2700 fluorescence spectrophotometer after being excited by a 980 nm laser source. The standard curves of IFE-IA were established by plotting the change of fluorescence intensity ($I = I - I_0$, where I and I_0 represent the fluorescence intensity at 657 nm in the presence and absence of benzothiostrubin) and the logarithm concentration of benzothiostrubin.

2.5. Analysis of Spiked Samples.

Paddy water, soil, corn, rice, and cucumber were collected from farms in Nanjing, China, and were shown to be benzothiostrubin-free by HPLC analysis with UV detector. The samples were homogenized and spiked with benzothiostrubin at the final concentrations of 20, 80, and 100 ng mL⁻¹ for paddy water; 100, 400, and 1000 ng g⁻¹ for soil and corn; 200, 500, and 1000 ng g⁻¹ for rice and cucumber. Paddy water was diluted 2 times with 2X buffer before analysis. Solid samples were extracted twice by vortexing for 3 min with 10 mL of BB containing 25% methanol, sonication for 15 min, and centrifugation at 4000 rpm for 5 min. The total supernatant was transferred and adjusted to 25 mL using BB. The concentration of benzothiostrubin was analyzed after appropriate dilution.

2.6. Practical Application.

Cucumber samples were collected from farms in Nanjing, China, where benzothiostrubin had been sprayed. The amounts of benzothiostrubin were detected by IFE-IA and HPLC simultaneously. The IFE-IA procedure was the same as for the spiked samples. Extraction procedure for HPLC analysis of benzothiostrubin in cucumber samples was reported previously.³⁷

3. RESULTS AND DISCUSSION

3.1. Design and Verification of the Peptides.

Dendrimer-like dimer and tetramer peptidomimetics were synthesized by using lysine as the scaffold, which is commonly used as dendrimer unit.⁴⁴ For conjugation of the peptides to

UCNPs, the carboxyl group at the C-terminal of the peptide did not seem to be suitable because of presence of glutamic acid (E) in the peptidomimetic (CSGLAEFMSC) sequence. The amino group at N-terminal is also unsuitable because dendrimer-like peptides have multiple N-terminals. In order to present peptidomimetic in monomer, dendrimer-like dimer and tetramer toward outside in a similar way, the N-terminals of peptides were acetylated, and an additional lysine was added at the C-terminal to provide an amino group in the side chain (Ac-CSGLAEFMSC, (Ac-CSGLAEFMSC)₂KK and ((Ac-CSGLAEFMSC)₂K)₂KK). Therefore, the monomer, dimer and tetramer peptidomimetics contained only one side chain amino group at the C-terminal.

All peptides were >95% pure as determined by HPLC-MS and measured *m/z* values were in good agreement with calculated mass (Table S1). In addition, the peptides were used as the substitutes for the analyte to compete with coating antigen in the indirect competitive ELISA (ic-ELISA). The results showed the OD₄₅₀ values were decreased in the presence of peptides (Figure S1).

3.2. Affinities of the Peptides toward mAb.

The affinities of different valence peptides toward the same mAb were determined by ITC through titrating peptides into mAb solution. The titration curves and binding constants are shown in Figure 1. The dendrimer-like dimer and tetramer had respectively 1.87-fold ($6.94 \times 10^5 \text{ M}^{-1}$, Figure 1B) and 13.6-fold ($5.06 \times 10^6 \text{ M}^{-1}$, Figure 1C) higher affinity for mAb, compared to monomer ($3.72 \times 10^5 \text{ M}^{-1}$, Figure 1A). Similarly, the absolute value of thermodynamic parameters namely binding enthalpy (ΔH) and entropy (ΔS) of dimer and tetramer were higher than monomer. The ΔH values (negative) indicate all the interactions were exothermic and the dendrimer-like tetramer has the strongest binding because of the largest absolute value of ΔH .²¹ The larger ΔS may be mainly due to the reduction of degrees of freedom caused by the oligo/polymerization of mAb and dendrimer-like tetramer. The negative value of ΔH and ΔS indicated that the binding process was driven by favorable enthalpy and unfavorable entropy.⁴⁵ The *c* value of monomer, dimer, and tetramer were in the range of 1 to 1000 (5.08, 2.26, and 12.40, respectively), pointing out that the results were of good quality.^{46,47}

ITC tests illustrated that dendrimer-like tetramer showed a markedly stronger binding toward mAb compared to monomer and dendrimer-like dimer. This seemed to be mainly due to the avidity factor associated with polyvalency of dendrimeric-like ligands masking low individual peptide affinity.^{14,18,48} Anyway, these results indicated that parallel multicopy ligands can increase the affinity for the target without changing the binding mode, because the availability of the binding domain of the ligands was not changed.²¹

3.3. Characterization of Probes.

3.3.1. Characterization of AuNFs and AuNF Probes.—As shown in Figure 2A, the diameter of monodisperse AuNSs was about 19 nm. The diameter of AuNFs was about 105 nm with many scattered intersecting subunits surrounding a solid core and exhibit a flowerlike shape according to SEM (Figure 2B).^{34,36} AuNF probe (mAb-AuNFs) was validated by spectroscopy and zeta potential. The UV-vis spectra showed that the absorbance

peak of AuNFs was 645 nm. The absorbance peak was red-shifted about 15 nm after labeling with mAb (Figure 2C). Besides, the zeta potential of AuNFs was changed from -51.32 ± 3.99 to -40.71 ± 3.78 mV after labeling with mAb. These results confirmed successful labeling of AuNFs surface with mAb.

3.3.2. Characterization of UCNP and UCNP Probes.—The morphology of the prepared UCNP was characterized by TEM. These nanoscale spheres were of regular spherical shape with an average size of 100 nm (Figure 2D). The XRD indicated that synthesized UCNP were of hexagonal phase (Figure 2E). FTIR spectroscopy verified that UCNP were surrounded with amino groups (Figure 2F). Peptide labeling of UCNP probes was confirmed by immunoreaction with antibenzothiothiobin mAb followed by goat antimouse IgG- HRP, which produced a colorimetric signal after introduction of substrate (Figure 2G). These results indicated that peptidomimetics were successfully conjugated to UCNP and maintained good activity.

3.4. Mechanism of the IFE-IA for the Detection of Benzothiothiobin.

The fluorescence emission spectrum of UCNP probes and absorption spectrum of AuNF probes are shown in Figure 3A, and an obvious spectrum overlap was observed at 657 nm. Such a spectrum overlap can be exploited in IFE and FRET, two equally significant fluorescence decay mechanisms, which are widely used for optical immunoassays.^{27,49} However, IFE is not a quenching process, it is just an attenuation of energy from donor by receptor in solution, while FRET is an electrodynamic phenomenon, which decreases the fluorescence lifetime due to the nonradiative excited-state energy transfer from fluorophore to quencher.²⁸ In our present study, fluorophore lifetime plots of UCNP probes in the presence and absence of AuNF probes were essentially the same (Figure 3B, $\tau = 393.5 \mu\text{s}$), which indicated the fluorescence decay mechanism is caused by IFE rather than FRET. In the IFE-IA, if there is no analyte (benzothiothiobin) in sample solution, the UCNP and AuNF probes would bind together by the specific reaction between mAb and peptidomimetic, which caused fluorescence of UCNP was absorbed by AuNFs (turn off). In contrast, benzothiothiobin competed with the UCNP probes to bind with AuNF probes to decrease the IFE and recovered fluorescence signal (turn on) (Scheme 1B).

3.5. Comparison of the Peptidomimetics in IFE-IAs.

Appropriate amount of probes are important for the sensitivity of immunoassay. In this competitive format immunoassay, fluorescence intensity decreased with the increasing volume of AuNF probes. When the volumes were equal or greater than $60 \mu\text{L}$ the fluorescence intensities reached plateau in the IFE-IAs based on monomer, dendrimer-like dimer and tetramer peptidomimetics (Figure 3C). Thus, $60 \mu\text{L}$ was selected as the optimal amount of AuNFs for the immunoassay. It is interesting to note that the plateau fluorescence intensity for dendrimer-like tetramer was the lowest, indicating that least free UCNP probes existed in the solution due to the highest affinity between mAb and dendrimer-like tetramer via the avidity effect. Besides, since the plateau fluorescence is the background fluorescence in the homogeneous immunoassays, lower plateau fluorescence may positively influence the sensitivity. As expected, the SC_{50} values of the IFE-IAs based on monomer, dimer and tetramer were 65.6, 31.3, and 11.4 ng mL^{-1} , respectively (Figure 3D). Compared to

monomer and dimer, the sensitivity of the IFE-IA was improved approximately 6 and 3 fold by using tetramer. Therefore, the dendrimer-like tetramer was used in all further experiments because of its higher sensitivity.

3.6. Sensitivity and Selectivity of IFE-IA.

3.6.1. Sensitivity.—The sensitivity of immunoassay is often improved by optimizing the working buffer. The parameters of working buffer including pH (6.4, 7.4, 8.4, 9.4), concentration of Na⁺ (0.1 M, 0.2 M, 0.3 M, 0.4 M) and methanol content (2.5, 5, 10, and 20%) were tested by the IFE-IA. The lower SC₅₀ and higher F_{\max}/SC_{50} were desirable. The optimal conditions of IFE-IA were pH 7.4, 0.1 M Na⁺ and 2.5% methanol (Figure S2).

Under the optimal conditions, the changes of fluorescence intensity with different concentrations of benzothiostrubin standard and the corrected curves are shown in Figure 4A. The SC₅₀, limit of detection (LOD) and linear range (SC₁₀ to SC₉₀) were 11.81 ± 0.72, 2.04, 2.04 to 106.17 ng mL⁻¹, respectively. The sensitivity (SC₅₀) of IFE-IA was better than competitive fluorescence immunoassay (FIA, IC₅₀ = 16.8 ng mL⁻¹) and noncompetitive FIA (SC₅₀ = 93.4 ng mL⁻¹) based on synthetic peptides (FITC-Ahx-CSGLAEFMSC and FITC-Ahx-CPDIWPTAWC).³⁷ Compared with other reported immunoassays for benzothiostrubin, the sensitivity of this assay was slightly lower than ic-ELISA (IC₅₀ = 7.55 ng mL⁻¹),³⁸ and approximately 10-fold lower than phage ELISAs (IC₅₀ = 0.94 ng mL⁻¹ for competitive phage ELISA, SC₅₀ = 2.27 ng mL⁻¹ for noncompetitive phage ELISA).⁹ It has been previously speculated that a high load of tracer molecules on the surface of phage may be responsible for higher sensitivity of phage ELISAs.² Although the IFE-IA did not show an outstanding advantage in sensitivity, it is able to detect benzothiostrubin in agricultural products according to the maximum residue limits (MRLs) of methoxyacrylate fungicides, such as azoxystrobin (0.5 mg kg⁻¹ for cucumber, 0.02 mg kg⁻¹ for corn, 0.5 mg kg⁻¹ for rice permitted in China, GB 2763–2016). Most importantly, the peptidomimetic isolated from the phage display library was successfully used to develop a homogeneous immunoassay with turn off-on model (positive readout), faster detection (1 h) and simpler operation (1 step) (Table 1). Therefore, dendrimer-like peptides are efficient substitutes of phage-borne peptides for the development of homogeneous immunoassays with simple and rapid detection procedures.

3.6.2. Selectivity.—The selectivity of IFE-IA was evaluated by measuring cross-reactivity (CR) with five structurally related benzothiostrubin analogues (pyraclostrobin, azoxystrobin, kresoxim-methyl, picoxystrobin and chloropiperidine ester). The analogues producing a 50% saturation of the signal were used to calculate the CR according to the formula: CR (%) = [SC₅₀ (benzothiostrubin)/SC₅₀ (analogue)] × 100. The CRs were less than 0.1%, which indicated the IFE-IA showed no CRs to analogues (Table 2). Compared with the ic-ELISA² and phage ELISA⁹ (CR = 0.34% for pyraclostrobin), the IFE-IA had higher selectivity for benzothiostrubin.

3.7. Recovery of Benzothiostrubin from Spiked Samples.

The dilution of sample extracts was performed to eliminate the matrix interferences on the immunoassay. As shown in Figure S3, the total dilution that eliminated matrix effects was 2-

fold for paddy water, 10-fold for soil, 20-fold for corn, and 40-fold for rice and cucumber. Under these dilutions, the average recoveries of benzothiostrubin in spiked paddy water, soil, corn, rice, and cucumber were in the range of 74.2%–105.4% with RSDs of 5.2%–11.9% (Table 3).

3.8. Validation with HPLC.

The real cucumber samples obtained from fields treated with benzothiostrubin were used for comparative study with IFE-IA and HPLC. The concentrations of benzothiostrubin detected by IFE-IA (112.28–931.11 ng g⁻¹) were in good agreement with values obtained by HPLC (87.50–957.31 ng g⁻¹) (Table S2). The *p* value (0.80) calculated by a Student's *t*-test was greater than 0.05, implying that the data obtained with IFE-IA and HPLC were not significantly different. In addition, there were good correlations between IFE-IA and HPLC (Figure 4B), because the slope value of correlation curve was very close to 1 (0.963). These results indicate that the presented IFE-IA is a reliable and accurate assay for the detection of benzothiostrubin in environmental and agricultural samples.

4. CONCLUSIONS

In this study, the cyclic peptidomimetics that bound specifically with antibenzothiostrubin mAb were designed and synthesized in the form of monomer, dendrimer-like dimer and tetramer, and applied to develop a homogeneous IFE-IAs with turn off-on model by using peptide-labeled UCNP as energy donor and mAb-labeled AuNPs as energy absorber. The dendrimer-like peptidomimetics (dimer and tetramer) were prepared by using lysine as scaffold, and the peptides (including monomer) were labeled with UCNP through the same amino group from side chain of an additional lysine at the C-terminal. The affinity between peptidomimetic and mAb increased significantly with increased valence (avidity effect), while the background fluorescence intensity of IFE-IA decreased at the same time, which resulted in the increased assay sensitivity. Therefore, the present work provides a new strategy for preparation of phage-free high affinity peptides to develop a nanoplatform for monitoring small molecules.

Supplementary Material

Refer to Web version on PubMed Central for supplementary material.

ACKNOWLEDGMENTS

This work was supported by the National Natural Science Foundation of China (Grant 31772194), the National Key Research and Development Program of China (Grant 2017YFF0210200), the National Institute of Environmental Health Sciences, Superfund Research Program (Grant P42 ES04699), and CSIC 149 UdelaR Uruguay.

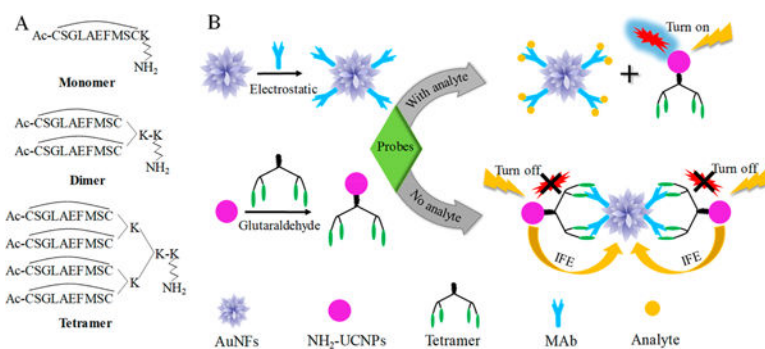
REFERENCES

- (1). Wang J; Liu ZP; Li GQ; Li J; Kim HJ; Shelver WL; Li QX; Xu T Simultaneous Development of both Competitive and Noncompetitive; Immunoassays for 2,2',4,4'-Tetrabromodiphenyl Ether Using; Phage-Displayed Peptides. *Anal. Bioanal. Chem.* 2013, 405, 9579–9583. [PubMed: 24096567]

- (2). Cardozo S; González-Techera A; Last JA; Hammock BD; Kramer K; Gonzalez-Sapienza G Analyte Peptidomimetics Selected from Phage Display Peptide Libraries: A Systematic Strategy for the Development of Environmental Immunoassays. *Environ. Sci. Technol.* 2005, 39, 4234–4241. [PubMed: 15984805]
- (3). Gonzalez-Techera A; Umpierrez-Failache M; Cardozo S; Obal G; Pritsch O; Last JA; Gee SJ; Hammock BD; Gonzalez-Sapienza G High-Throughput Method for Ranking the Affinity of Peptide Ligands Selected from Phage Display Libraries. *Bioconjugate Chem.* 2008, 19, 993–1000.
- (4). Kim HJ; Gonzalez-Techera A; Gonzalez-Sapienza G; Ahn KC; Gee SJ; Hammock BD Phage-Borne Peptidomimetics Accelerate the Development of Polyclonal Antibody-Based Heterologous Immunoassays for the Detection of Pesticide Metabolites. *Environ. Sci. Technol.* 2008, 42, 2047–2053. [PubMed: 18409635]
- (5). Ding Y; Hua XD; Chen H; Liu FQ; Gonzalez-Sapienza G; Wang MH Recombinant Peptidomimetic-Nano Luciferase Tracers for Sensitive Single-Step Immunodetection of Small Molecules. *Anal. Chem.* 2018, 90, 2230–2237. [PubMed: 29280616]
- (6). Gonzalez-Techera A; Kim HJ; Gee SJ; Last JA; Hammock BD; Gonzalez-Sapienza G Polyclonal Antibody-Based Noncompetitive Immunoassay for Small Analytes Developed with Short Peptide Loops Isolated from Phage Libraries. *Anal. Chem.* 2007, 79, 9191–9196. [PubMed: 17973501]
- (7). Wegner KD; Linden S; Jin Z; Jennings TL; Khoulati R e.; van Bergen en Henegouwen PMP; Hildebrandt N Nanobodies and Nanocrystals: Highly Sensitive Quantum Dot-Based Homogeneous FRET Immunoassay for Serum-Based EGFR Detection. *Small* 2014, 10, 734–740. [PubMed: 24115738]
- (8). Lim SL; Ichinose H; Shinoda T; Ueda H Noncompetitive Detection of Low Molecular Weight Peptides by Open Sandwich Immunoassay. *Anal. Chem.* 2007, 79, 6193–6200. [PubMed: 17636882]
- (9). Hua XD; Zhou LL; Feng L; Ding Y; Shi HY; Wang LM; Gee SJ; Hammock BD; Wang MH Competitive and Noncompetitive Phage Immunoassays for the Determination of Benzothiostrubin. *Anal. Chim. Acta* 2015, 890, 150–156. [PubMed: 26347177]
- (10). Rossotti MA; Carlomagno M; Gonzalez-Techera A; Hammock BD; Last J; Gonzalez-Sapienza G Phage Anti-Immunoassay for Clomazone: Two-Site Recognition Increasing Assay Specificity and Facilitating Adaptation into an On-Site Format. *Anal. Chem.* 2010, 82, 8838–8843. [PubMed: 20886819]
- (11). Valcourt DM; Harris J; Riley RS; Dang M; Wang JX; Day ES Advances in Targeted Nanotherapeutics: From Bioconjugation to Biomimicry. *Nano Res.* 2018, 11, 4999–5016. [PubMed: 31772723]
- (12). Yeh CY; Hsiao JK; Wang YP; Lan CH; Wu HC Peptide-Conjugated Nanoparticles for Targeted Imaging and Therapy of Prostate Cancer. *Biomaterials* 2016, 99, 1–15. [PubMed: 27209258]
- (13). Vanrell L; Gonzalez-Techera A; Hammock BD; Gonzalez-Sapienza G Nanopeptamers for the Development of Small-Analyte Lateral Flow Tests with a Positive Readout. *Anal. Chem.* 2013, 85, 1177–1182. [PubMed: 23214940]
- (14). Wang P; Wu J; Di CX; Zhou R; Zhang H; Su PR; Xu C; Zhou PP; Ge YS; Li D; Liu WS; Tang Y A Novel Peptide-Based Fluorescence Chemosensor for Selective Imaging of Hydrogen Sulfide both in Living Cells and Zebrafish. *Biosens. Bioelectron.* 2017, 92, 602–609. [PubMed: 27829566]
- (15). Lei YH; Hu TH; Wu XS; Wu Y; Bao QC; Zhang LS; Xia H; Sun HP; You QD; Zhang XJ Affinity-Based Fluorescence Polarization Assay for High-Throughput Screening of Prolyl Hydroxylase 2 Inhibitors. *ACS Med. Chem. Lett.* 2015, 6, 1236–1240. [PubMed: 26713111]
- (16). Ding Y; Hua XD; Du M; Yang Q; Hou LN; Wang LM; Liu FQ; Gonzalez-Sapienza G; Wang MH Recombinant, Fluorescent, Peptidomimetic Tracer for Immunodetection of Imidacloprid. *Anal. Chem.* 2018, 90, 13996–14002.
- (17). Lassabe G; Rossotti M; Gonzalez-Techera A; Gonzalez-Sapienza G Recombinant Streptavidin Nanopeptamer Anti-Immunoassay for Noncompetitive Detection of Small Analytes. *Anal. Chem.* 2014, 86, 5541–5546. [PubMed: 24797274]

- (18). Knez K; Noppe W; Geukens N; Janssen KPE; Spasic D; Heyligen J; Vriens K; Thevissen K; Cammue BPA; Petrenko V; Ulens C; Deckmyn H; Lammertyn J Affinity Comparison of p3 and p8 Peptide Displaying Bacteriophages Using Surface Plasmon Resonance. *Anal. Chem.* 2013, 85, 10075–10082.
- (19). Li LY; Orner BP; Huang T; Hinck AP; Kiessling LL Peptide Ligands That Use a Novel Binding Site to Target both TGF- β Receptors. *Mol. BioSyst.* 2010, 6, 2392–2402. [PubMed: 20890540]
- (20). Helms BA; Reulen SWA; Nijhuis S; de Graaf-Heuvelmans PTHM; Merkx M; Meijer EW High-Affinity Peptide-Based Collagen Targeting Using Synthetic Phage Mimics: from Phage Display to Dendrimer Display. *J. Am. Chem. Soc.* 2009, 131, 11683–11685. [PubMed: 19642697]
- (21). Dudak FC; Kilic N; Demir K; Yasar F; Boyaci IH Enhancing the Affinity of SEB-Binding Peptides by Repeating Their Sequence. *Biopolymers* 2012, 98, 145–154. [PubMed: 22733526]
- (22). Weissleder R; Kelly K; Sun EY; Shtatland T; Josephson L Cell-Specific Targeting of Nanoparticles by Multivalent Attachment of Small Molecules. *Nat. Biotechnol* 2005, 23, 1418–1423. [PubMed: 16244656]
- (23). Kitov PI; Sadowska JM; Mulvey G; Armstrong GD; Ling H; Pannu NS; Read RJ; Bundle DR Shiga-Like Toxins are Neutralized by Tailored Multivalent Carbohydrateligands. *Nature* 2000, 403, 669–672. [PubMed: 10688205]
- (24). Hu Q; Chen Q; Yan XY; Ding BM; Chen DW; Cheng LF Chondrocyte Affinity Peptide Modified PAMAM Conjugate as a Nanoplatform for Targeting and Retention in Cartilage. *Nanomedicine* 2018, 13, 749–767. [PubMed: 29528264]
- (25). Yu XZ; Wen K; Wang ZH; Zhang XY; Li CL; Zhang SX; Shen JZ A General Bioluminescence Resonance Energy Transfer Homogeneous Immunoassay for Small Molecules Based on Quantum Dots. *Anal. Chem.* 2016, 88, 3512–3520. [PubMed: 26948147]
- (26). Bagdeli S; Rezayan AH; Taheri RA; Kamali M; Hosseini M Morteza Hosseini FRET-Based Immunoassay Using CdTe and AuNPs for the Detection of OmpW Antigen of *Vibrio Cholera*. *J. Lumin.* 2017, 192, 932–939.
- (27). You H; Hua X; Feng L; Sun N; Rui Q; Wang L; Wang M Competitive Immunoassay for Imidacloprid Using Upconversion Nanoparticles and Gold Nanoparticles as Labels. *Microchim. Acta* 2017, 184, 1085–1092.
- (28). Chen S; Yu YL; Wang JH Inner Filter Effect-Based Fluorescent Sensing Systems: A Review. *Anal. Chim. Acta* 2018, 999, 13–26. [PubMed: 29254563]
- (29). Jin X; Sang YT; Shi YH; Li YG; Zhu XF; Duan PF; Liu MH Optically Active Upconverting Nanoparticles with Induced Circularly Polarized Luminescence and Enantioselectively Triggered Photopolymerization. *ACS Nano* 2019, 13, 2804–2811. [PubMed: 30688444]
- (30). Si FF; Zou RB; Jiao SS; Qiao XS; Guo YY; Zhu GN Inner Filter Effect-Based Homogeneous Immunoassay for Rapid Detection of Imidacloprid Residue in Environmental and Food Samples. *Ecotoxicol. Environ. Saf.* 2018, 148, 862–868.
- (31). Wang H; Li YK; Yang M; Wang P; Gu YQ FRET-Based Upconversion Nanoprobe Sensitized by Nd³⁺ for the Ratiometric Detection of Hydrogen Peroxide in Vivo. *ACS Appl Mater. Interfaces* 2019, 11, 7441–7449. [PubMed: 30673225]
- (32). Sabri T; Pawelek PD; Capobianco JA Dual Activity of Rose Bengal Functionalized to Albumin-Coated Lanthanide-Doped Upconverting Nanoparticles: Targeting and Photodynamic Therapy. *ACS Appl. Mater. Interfaces* 2018, 10, 26947–26953.
- (33). Pilch A; Wurth C; Kaiser M; Wawrzynczyk D; Kurnatowska M; Arabasz S; Prorok K; Samoc M; Streck W; Resch-Genger U; Bednarkiewicz A Shaping Luminescent Properties of Yb³⁺ and Ho³⁺ Co-Doped Upconverting Core-Shell Beta-NaYF₄ Nanoparticles by Dopant Distribution and Spacing. *Small* 2017, 13, 1701635.
- (34). Kong DS; Jin R; Zhao X; Li HX; Yan X; Liu FM; Sun P; Gao Y; Liang XS; Lin YH; Lu GY Protein-Inorganic Hybrid Nanoflower-Rooted Agarose Hydrogel Platform for Point-of-Care Detection of Acetylcholine. *ACS Appl. Mater. Interfaces* 2019, 11, 11857–11864.
- (35). Xie JP; Zhang QB; Lee JY; Wang DI The Synthesis of SERS-Active Gold Nanoflower Tags for in Vivo Applications. *ACS Nano* 2008, 2, 2473–2480. [PubMed: 19206281]

- (36). Xiao ZY; Xu CT; Jiang XH; Zhang WL; Peng YX; Zou RJ; Huang XJ; Liu Q; Qin ZY; Hu JQ Hydrophilic Bismuth Sulfur Nanoflower Superstructures with an Improved Photothermal Efficiency for Ablation of Cancer Cells. *Nano Res.* 2016, 9, 1934–1947.
- (37). Chen H; Yang Q; Ding Y; Vasylieva N; Bever CS; Hua XD; Wang MH; Hammock BD Competitive and Non-competitive Immunoassays for the Detection of Benzothiostrubin Using Magnetic Nanoparticles and Fluorescein Isothiocyanate-Labeled Peptides. *Anal. Bioanal. Chem.* 2019, 411, 527–535. [PubMed: 30478514]
- (38). Yuan YL; Hua XD; Li M; Yin W; Shi HY; Wang MH Development of a Sensitive Indirect Competitive Enzyme-Linked Immunosorbent Assay Based on the Monoclonal Antibody for the Detection of Benzothiostrubin Residue. *RSC Adv.* 2014, 4, 24406–24411.
- (39). Nieves RA; Ellis RP; Todd RJ; Johnson TJA; Grohmann K; Himmel ME Visualization of *Trichoderma Reesei* Cellobiohydrolase I and Endoglucanase Ion Aspen Cellulose by Using Monoclonal Antibody-Colloidal Gold Conjugates. *Appl. Environ. Microbiol.* 1991, 11, 3163–3170.
- (40). Maiorano G; Sabella S; Sorce B; Brunetti V; Malvindi MA; Cingolani R; Pompa PP Effects of Cell Culture Media on the Dynamic Formation of Protein? Nanoparticle Complexes and Influence on the Cellular Response. *ACS Nano* 2010, 4, 7481–7491. [PubMed: 21082814]
- (41). Sun YJ; Chen Y; Tian LJ; Yu Y; Kong XG; Zhao JW; Zhang H Controlled Synthesis and Morphology Dependent Upconversion Luminescence of NaYF₄:Yb, Er Nanocrystals. *Nanotechnology* 2007, 18, 275609.
- (42). Stalder K; Stober W Haemolytic Activity of Suspensions of Different Silica Modifications and Inert Dusts. *Nature* 1965, 207, 874–875. [PubMed: 4287340]
- (43). Hua XD; You HJ; Luo PW; Tao ZX; Chen H; Liu FQ; Wang MH Upconversion Fluorescence Immunoassay for Imidaclothiz by Magnetic Nanoparticle Separation. *Anal. Bioanal. Chem.* 2017, 409, 6885–6892. [PubMed: 28975377]
- (44). Petersen JF; Tortzen CG; Pittelkow M; Christensen JB Synthesis and Properties of Chiral Internally Branched PAMAM-Dendrimers. *Tetrahedron* 2015, 71, 1109–1116.
- (45). Xiao CQ; Lai L; Zhang L; Wang SY; Yuan S; Xu ZQ; Liu Y Spectroscopic and Isothermal Titration Calorimetry Studies of Binding Interactions Between Aarbon Nanodots and Serum Albumins. *J. Solution Chem.* 2018, 47, 1438–1448.
- (46). El Harrou M; Parody-Morreale A Measurement of Biochemical Affinities with a Gill Titration Calorimeter. *Anal. Biochem.* 1997, 254, 96–108. [PubMed: 9398351]
- (47). McKinnon IR; Fall L; Parody-Morreale A; Gill SJ A Twin Titration Microcalorimeter for the Study of Biochemical Reactions. *Anal. Biochem.* 1984, 139, 134–139. [PubMed: 6742425]
- (48). Fagerlund A; Myrset AH; Kulseth MA Construction and Characterization of a 9-mer Phage Display pVIII-Library with Regulated Peptide Density. *Appl. Microbiol. Biotechnol.* 2008, 80, 925–936. [PubMed: 18716770]
- (49). Lassabe G; Kramer K; Ha mmock BD; Gonzalez-Sapienza G; Gonzalez-Techera A Noncompetitive Homogeneous Detection of Small Molecules Using Synthetic Nanopeptamer Based Luminescent Oxygen Channeling. *Anal. Chem.* 2018, 90, 6187–6192. [PubMed: 29694028]



Scheme 1. (A) Schematic Diagrams of Dendrimer-Like Peptidomimetics and (B) IFE-IA Based on Peptidomimetics-Conjugated UCNP and mAbs-Labeled AuNFs

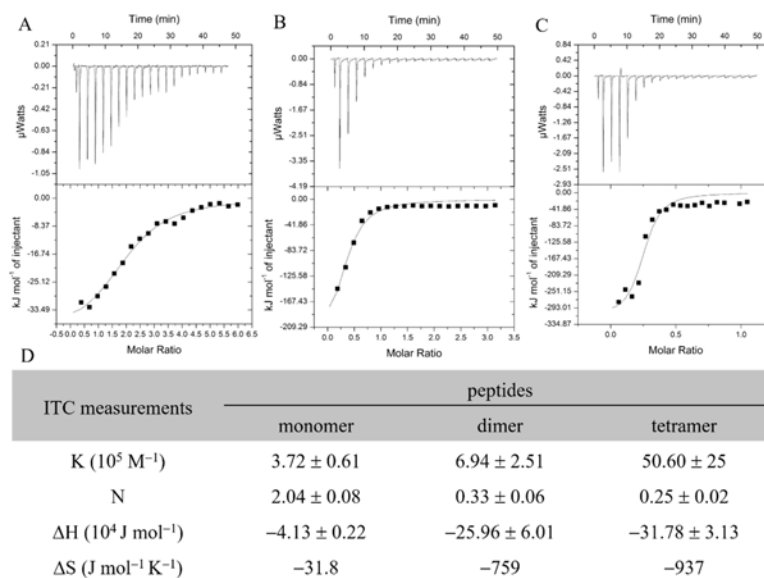


Figure 1. Affinities fitted curves between (A) monomer, (B) dendrimer-like dimer, and (C) dendrimer-like tetramer peptidomimetics and mAb by ITC. D) Binding thermodynamic parameters for ITC measurements.

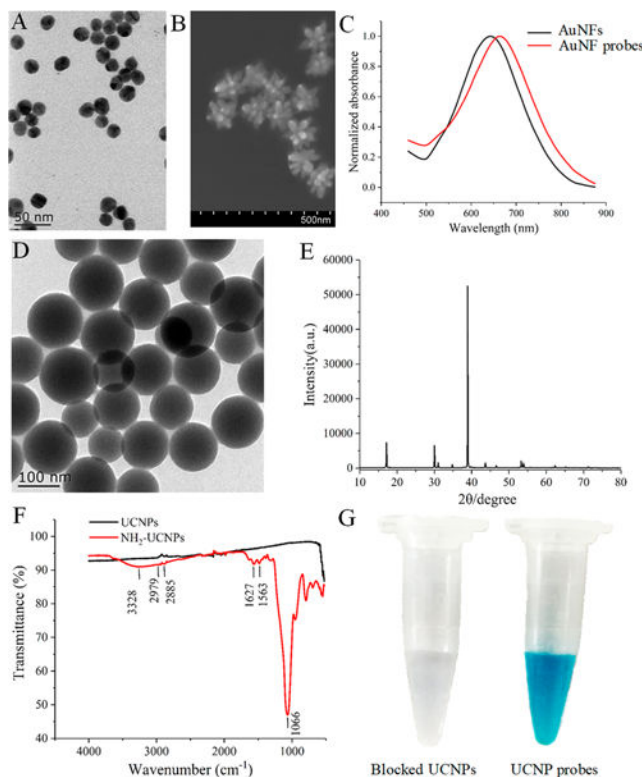


Figure 2.

(A) TEM image of gold seeds, (B) SEM image of AuNFs, (C) The surface plasmon resonance (SPR) bands of AuNF and AuNF probes. (D) TEM image of UCNPs, (E) The XRD of UCNPs, (F) FTIR spectroscopy of UCNPs and amino-modified UCNPs. Absorption band at 1089 cm^{-1} is due to stretching vibration of Si–O groups. The two absorption peaks at 3382 and 1633 cm^{-1} are attributed to stretching and bending vibration bands of O–H and/or N–H groups. Asymmetric and symmetric stretching vibrations of CH_2 groups distributed in 2988 and 2890 cm^{-1} . All of the above peaks indicate that UCNPs were successfully modified with amino groups, (G) Identification of tetramer peptidomimetics UCNP probes by goat antimouse IgG-HRP (the results of monomer and dimer peptidomimetics were essentially the same).

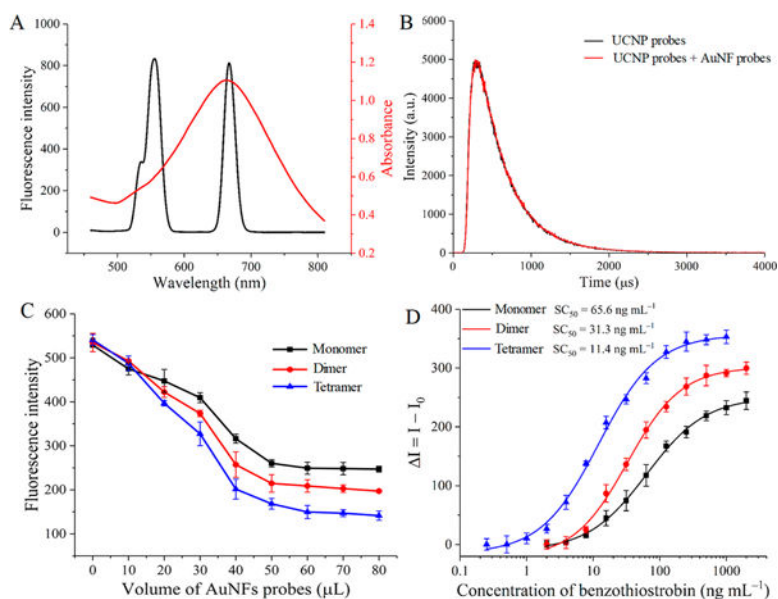


Figure 3.

(A) Fluorescence emission spectrum of tetramer peptidomimetics UCNP probes and absorption spectrum of AuNF probes. (B) Fluorophore lifetime of tetramer peptidomimetics UCNP probes and their mixture with AuNF probes. The results of monomer and dimer peptidomimetics were essentially the same. (C) Fluorescence intensity with different volume of AuNF probes, (D) Standard curves of IFE-IAs based on monomer, dimer, and tetramer peptidomimetics. Each point represents the average of three repetitions.

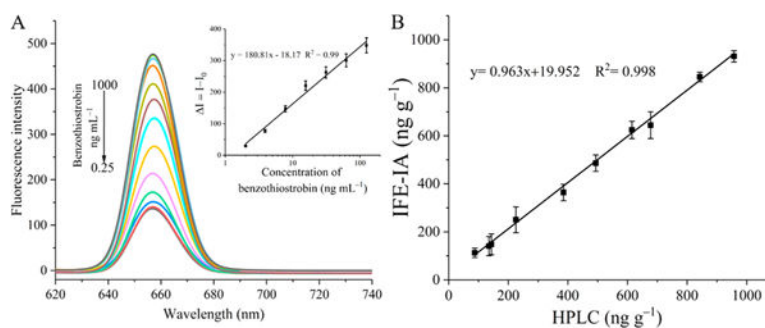


Figure 4.

(A) Fluorescence intensity changes with different concentrations of benzothiostrubin and corrected curve of IFE-IA. (B) Correlations between the IFE-IA and HPLC data. Ten authentic cucumber samples were analyzed by IFE-IA and HPLC simultaneously; the line equation and correlation coefficient obtained from the linear regression are shown. Each point represents the average of three repetitions.

Table 1. Comparison of Previous Immunoassays and IFE-IA for the Detection of Benzothiothrobin

methods	IC ₅₀ or SC ₅₀ (ng MI ⁻¹)	LOD (ng mL ⁻¹)	detection range (ng mL ⁻¹)	time (h)	step	ref
ic-ELISA	7.55	0.43	0.43–54	5.08 ^a	six	38
phage ELISAs	0.94	0.22	0.22–3.94	5.75		9
	2.27	1.11	1.11–4.62			
FIAs	16.8	1.0	1.0–759.9	1.2	two	37
	93.4	5.9	5.9–788.2			
IFE-IA	11.81	2.04	2.04–106.17	1	one	this work

^aThe incubation for overnight at 4 °C was replaced by 2 h at 37 °C to calculate the analysis time.

Table 2.

CRs of the Five Analogues Structurally Related to Benzo[thio]strobin by IFE-IA

compound	chemical structure	SC ₅₀ (ng mL ⁻¹)	CR (%)
benzo[thio]strobin		11.81	100
pyraclostrobin		>12000	<0.1
azoxystrobin		>12000	<0.1
kresoxim-methyl		>12000	<0.1
picoxystrobin		>12000	<0.1
Chloropiperidine ester		>12000	<0.1

Table 3.Average Recoveries of Benzothiostrubin from Spiked Samples by IFE-IA ($n = 3$)

sample	spiked (ng mL ⁻¹ or ng g ⁻¹)	average recovery (%)	RSD (%)
paddy water	20	88.0	5.7
	80	105.4	9.9
	200	74.2	7.9
soil	100	76.1	10.3
	400	90.6	8.4
	1000	88.5	11.9
corn	100	80.9	5.2
	400	104.7	6.4
	1000	94.9	7.5
cucumber	200	102.1	10.9
	500	87.7	7.2
	1000	100.9	8.1
rice	200	81.1	6.7
	500	77.6	10.3
	1000	94.9	11.1